Strong-strong simulation on the beam-beam effect in a linac-ring B factory

Rui Li and Joseph J. Bisognano
Continuous Electron Beam Accelerator Facility, 12000 Jefferson Avenue, Newport News, Virginia 23606
(Received 16 April 1993)

Since the inherently low emittance required by the linac-ring B factory implies high disruption for the linac bunch, previous investigations of the beam-beam tune-shift limit may not apply. A strong-strong simulation scheme was developed based on a macroparticle model to simulate beam-beam interaction in this situation self-consistently. Included in the ring dynamics are linear betatron oscillations and synchrotron motion, as well as transverse and longitudinal damping and quantum excitation. As a benchmarking test, the coherent quadrupole effect in a ring-ring collider was observed by the simulation. The code was then used to study the stability of the storage-ring bunch in a linac-ring collider and yielded strong synchrobetatron coupling due to the deep envelope modulation of the linac bunch. It was, however, observed that when initial conditions for the linac beam were properly chosen to match the focusing provided by the ring beam at IP, the beam-beam tune-shift limit of the ring beam could be comparable to that of a ring-ring collider.

PACS number(s): 41.85.−p, 41.75.−i

I. INTRODUCTION

An asymmetric e^+e^- collider with a 10-GeV center-of-mass energy can be used as a B factory to study the CP violation in the B-meson system. The luminosity required for this purpose should have a value of $\mathcal{L} > 10^{33}\ \mathrm{cm}^{-2}\,\mathrm{s}^{-1}$, which is much higher than the currently observed luminosity on existing machines. For the collision of transversely Gaussian distributed e^+e^- bunches, the luminosity is given by

$$\mathcal{L} = \frac{N_+ N_- f_c}{2\pi\sqrt{\sigma_{x+}^2+\sigma_{x-}^2}\sqrt{\sigma_{y+}^2+\sigma_{y-}^2}}, \tag{1.1}$$

where $N_\pm$ are the numbers of particles per bunch; f_c, the bunch collision frequency; and $\sigma_{x\pm}$ and $\sigma_{y\pm}$, the horizontal and vertical bunch sizes, respectively. The vertical beam-beam tune shift for the positron bunch, which characterizes the vertical focusing effect of the electron bunch on the approaching positron particles, is defined by

$$\xi_{y+} = \frac{r_0 N_- \beta_{y+}^*}{2\pi\gamma_+\sigma_{y-}(\sigma_{x-}+\sigma_{y-})}, \tag{1.2}$$

where γ_+ and β_{y+}^* are the Lorentz factor and the vertical beta function at IP for the positron bunch, and r_0, the classical electron radius. The other three beam-beam tune-shift parameters can be obtained by the replacements $x \leftrightarrow y$ and/or $+ \leftrightarrow -$. According to Eq. (1.1), one needs to increase the collision frequency f_c and the charge intensities for both e^+ and e^- bunches in order to reach the goal of $\mathcal{L} = 10^{33-34}\ \mathrm{cm}^{-2}\mathrm{s}^{-1}$. However, the intrinsic feature of nonlinearity in the beam-beam interaction sets a limit on the achievable beam-beam tune shift, which is typically around 0.06 for ring-ring colliders, above which the beam will start to blow up to a larger equilibrium bunch size in a few damping times. This beam-beam effect is primarily responsible for the limitation on the observed luminosity.

The idea of a linac-ring collider is proposed [1], such that the beam from the linac is not recycled after each collision. Typically, in these scenarios, the electron beam is provided by the linac, and the harder-to-produce positron beam is accumulated in the storage ring. In the following, therefore, the linac particles are electrons; the storage-ring particles, positrons. As a result, the charge intensity for the e^+ bunch is no longer restricted by the beam-beam tune-shift limit for ξ_{y-}. It is expected that this will enlarge the parameter space available for such a colliding scheme that is designed to accomplish the luminosity goal. An additional feature of a linac-ring B factory is that, at the required high luminosity, the relatively low-average-beam-current capability of linacs compared to a storage ring implies low emittance. The consequently high positron charge density together with the low γ_- lead to high disruption for the electrons. The disruption parameter D_{y-} is defined as the ratio of the positron bunch length to the electron vertical focal length

$$D_{y-} = \frac{\sigma_{z+}}{f_{y-}} = \frac{2r_0 N_+ \sigma_{z+}}{\gamma_-\sigma_{y+}(\sigma_{x+}+\sigma_{y+})}. \tag{1.3}$$

For several given lists [2,3] of design parameters, the parameter D_{y-} is of the order of 100, indicating that the electron particles oscillate through the positron bunch during each collision. The beam-beam dynamics experienced by the positron bunch is therefore disparate from that in a ring-ring collider, and the beam-beam tune-shift limit for ξ_{y+} is not necessarily equal to the familiar number 0.06. Thus, to be confident of the linac-ring B factory performance estimates, one needs to study the stability of the positron beam in the storage ring when it undergoes collisions with highly disrupted electron bunches.

The simulation for the beam-beam effect in a linac-ring B factory should be strong-strong since we are interested in the evolution of the strong (positron) beam in the pro-

cess of its interaction with the relatively weak (electron) beam. In this study, a macroparticle model is employed to simulate the beam-beam interaction. This model was previously used [4] to display the high disruption effect on the electrons for a single collision of two round beams. Here an extended model is used to accommodate the interaction of elliptical beams. Care has been taken in choosing the sizes of the macroparticles and the number of macroparticles necessary in each beam in order to obtain statistically reliable results. The dynamics of the storage ring beam is studied by tracking the macroparticles in the ring over a number of damping times, where each turn comprises the beam-beam interaction at the IR, the linear betatron oscillation, and the synchrotron motion, as well as the radiation damping and the quantum fluctuation effect.

In Sec. II, we describe in detail the macroparticle model for the beam-beam interaction. Included in the Appendix are also some analytical estimates of the effects of the sizes and the numbers of macroparticles used in the simulation of the calculations of the beam-beam forces and luminosities. As a benchmarking test, the simulation scheme was used to manifest the coherent quadrupole effect in ring-ring colliders for round beams. The reasonable agreement of our calculation with the existing results [5,6] is shown in Sec. III. The beam-beam effect of a ring-ring collider using parameters given in the Positron-Electron Project (Stanford University) (PEP) B factory proposal [7–9] is studied in Sec. IV. We then proceed in Sec. V to investigate the behavior of the positron beam in a linac-ring B factory. Strong synchrobetatron coupling in the motion of positron particles has been observed, which is induced by the pinches of the highly disrupted electron bunches during collisions. It is shown that the beam-beam limit for the parameter ξ_{y+} can be made comparable to that of a ring-ring collider when the electron bunches enter into the IR with properly matched [3] initial conditions. The effect of jitter in the linac beam is discussed in Sec. VI.

II. SIMULATION

In this section, the macroparticle model [10] used for the strong-strong beam-beam interaction is discussed. The overall layout of the program, including the simulation of the dynamics undergone by the bunches in the storage ring, is also presented.

A. Beam-beam interaction model

At the IR of an e^+e^- collider, the two relativistic beams exert Lorentz forces on each other only in the transverse directions. The longitudinal motion of all the particles in a bunch is then uniform during a collision process. This allows us to divide each bunch longitudinally into many slices; the width of a slice corresponds to the longitudinal step size over which the charged particles are advanced in the collisions. Here, the number of slices should be sufficient to describe the beam-beam effect due to the longitudinal variation of the charge distributions. In the simulation, each slice is populated with macroparticles. The macroparticles in the two colliding beams experience mutual forces only when their corresponding slices overlap. Since the number of macroparticles is limited by computer capacity, shot noise often appears in the simulation results, and one needs to assign finite sizes to the macroparticles to suppress this effect. This finite size macroparticle model does not impose any restriction on the charge distributions of the beams under study.

In the code, the force on each macroparticle is computed by direct Coulomb sum,

$$\mathbf{F}(\mathbf{r}_i^{(1)}) = \sum_m \mathbf{f}(\mathbf{r}_i^{(1)} - \mathbf{r}_m^{(2)}), \tag{2.1}$$

where $\mathbf{F}(\mathbf{r}_i^{(1)})$ is the total force on the ith macroparticle in beam 1 at a given time step, and $\mathbf{f}(\mathbf{r}_i^{(1)} - \mathbf{r}_m^{(2)})$ is the force acting on the ith macroparticle in beam 1 by the mth macroparticle in beam 2 which lies in the same longitudinal interval as the former one. From the two-dimensional electrostatics, it has been shown [11] that the luminosity for each pair of interacting macroparticles is related with their mutual force by

$$\mathcal{L}_{im} = \frac{\epsilon_0}{e^2} \nabla \cdot \mathbf{f}(\mathbf{b}), \tag{2.2}$$

where $\mathbf{b} = \mathbf{r}_i^{(1)} - \mathbf{r}_m^{(2)}$ is the displacement of the centers of the two macroparticles. The total luminosity can then be obtained by the sum over the luminosity for each interaction pair at each time step, namely,

$$\mathcal{L} = \sum_{i,m} \mathcal{L}_{im}. \tag{2.3}$$

The aspect ratios for colliding beams in different designs vary in a wide range of values. For the general application of the simulation, the macroparticles are set to be Gaussian in charge distribution, with aspect ratio comparable to the designed beam aspect ratio. This will provide a better overlapping of macroparticles and hence reduce the spurious collisional effects (see the Appendix). Here, the electric fields on a two-dimensional grid, generated by a Gaussian macroparticle with given aspect ratio, are obtained from the well-known expression in terms of the complex error functions [12] and stored in a table. The mutual force for each interaction pair of macroparticles is then readily calculated by interpolating data from the lookup table. This is actually not the force between two charge distributions, but rather the forces of one elliptic Gaussian macroparticle on a point charge, as if all the charge in the second macroparticle were at the center of the macroparticle. More discussion on the simulation scheme can be found in the Appendix.

In certain situations, the sizes and the aspect ratio of the beam envelope evolve with time. This is particularly true in the linac-ring collision processes, where the electron bunches experience the pinching effect in each collision, and the positron bunches enlarge in several damping times. Therefore, the modeling of the force generated by each slice of a bunch should be treated separately, with the sizes of the macroparticles in each slice varied pro-

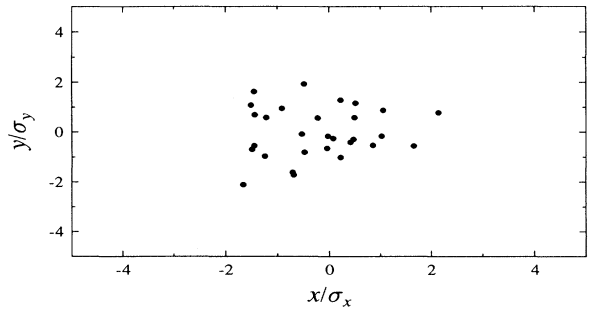

FIG. 1. Transverse Gaussian distribution simulated by 29 macroparticles.

portionally as the rms sizes of the corresponding slice evolve in each step of a collision. This will assure the proper description of the pinching effects. The ratio of the macroparticle size to the corresponding slice size is chosen to be $r = 0.5$ (see also the Appendix).

The finite macroparticle size plays the role of screening out the high-frequency shot-noise effect in the force calculation. Nonetheless, due to the finite number of macroparticles in each slice, it is inevitable to have residual fluctuations of the distribution of macroparticles around the ideal physical distribution. In the case when the overall charge distribution for a bunch in the storage ring changes slowly compared to the revolution period, the macroparticles in the bunch simulate different ensembles of the charge distribution in successive collisions due to their betatron motion in the ring. The average of the luminosities for these successive collisions then corresponds to the average over a certain number of ensembles and thus better simulates the true physical quantity. Reliable results should be insensitive to different random seeds, and their qualitative behavior should not change along with the increase of the number of macroparticles used in the simulation.

In Fig. 1, the centers of 29 macroparticles are displayed, which simulate a Gaussian charge distribution with aspect ratio $R = 3.93$. The macroparticles have the same aspect ratio as the bunch, but half the size. The total forces generated by these macroparticles are shown in Fig. 2 as the dotted curves, which are compared to the solid curves obtained analytically for the forces generated by a continuous Gaussian charge distribution. One can see that the high-frequency components of shot noise are suppressed by choosing finite sizes for the macroparticles. However, this is accomplished at the cost of equivalently larger bunch sizes for the calculated forces, as described by Eq. (A7). This effect explains the lower peak values for the calculated forces compared to the analytical results. Residual deviations for all the moments of distribution can also be seen in Fig. 2.

Comparisons of simulation results using different numbers of macroparticles are shown in Figs. 3 and 4. In Fig. 3 we use $N_{m-} = 360$ macroparticles for the electron bunch and $N_{m+} = 1000$ macroparticles for the positron bunch. The electron bunch accelerated by a linac collides at IR with the positron bunch in the storage ring. The two bunches initially have the same transverse bunch sizes. After 3000 turns, the positron bunch enlarges in the vertical direction as a result of beam-beam interaction. The equilibrium beam profiles right before the 3000th collision in the Y-Z plane are shown in Fig. 3(a), and the dependence of the blowup factor on the number of revolutions of the positron bunch in the ring is shown in Fig. 3(b). The same calculation was carried out for $N_{m-} = 1440$ and $N_{m+} = 4000$. It turns out that the average equilibrium vertical bunch size in Fig. 3(b) agrees reasonably with that in Fig. 4(b), even though the result in the former plot has more fluctuations than that in the latter one—the expected consequence of a smaller number of macroparticles being used for the simulation. Reducing the sizes of macroparticles will require an increase of the number of macroparticles used for the simulation and thus also of the computer time consumed. Such tests have been done, yielding results quantitatively depending on the macroparticle sizes according to Eq. (A7). Such dependence is insensitive as long as Eq. (A8) is satisfied.

B. Layout of the program

To create a good picture of the beam dynamics, we start with the electron and positron bunches located at

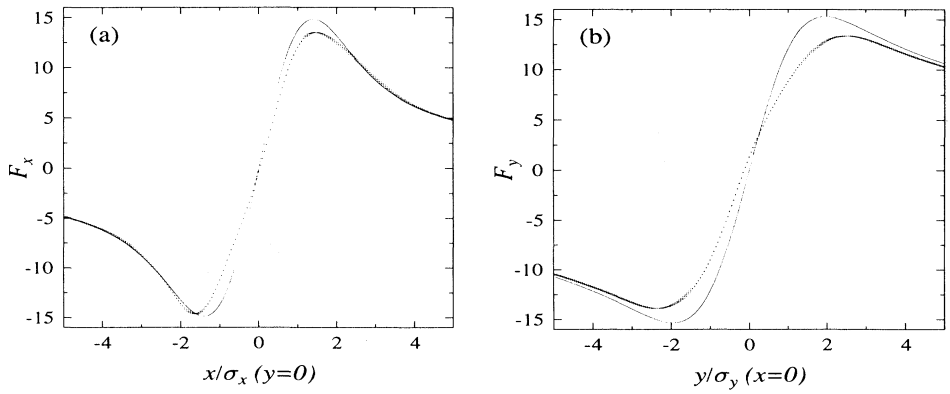

FIG. 2. Force calculated by macroparticle model (dotted curves) compared to analytical results (solid curves) for the distribution in Fig. 1.

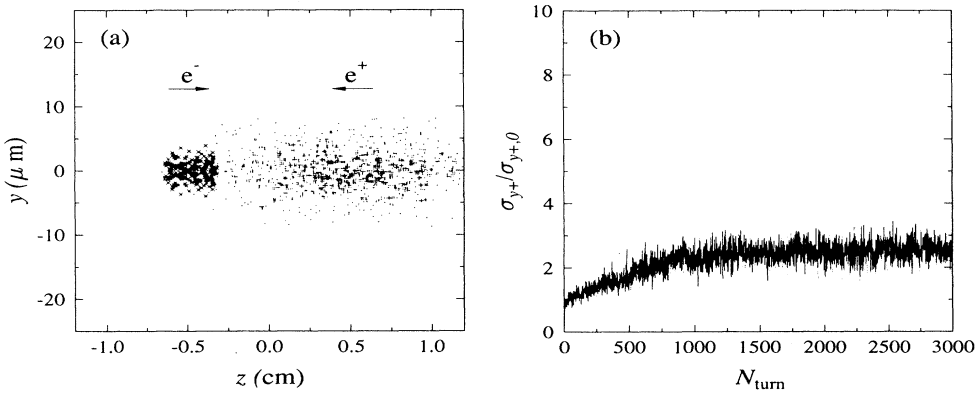

FIG. 3. Simulation results for (a) beam profiles before the 3000th collision and (b) verticle beam blowup factor vs number of turns. Here the number of macroparticles $N_{m-} = 360$ is used for the electron bunch and $N_{m+} = 1000$ for the positron bunch.

the precollision positions. The two bunches are then taken through each other and undergo the beam-beam interaction as described previously. In the case of the linac-ring colliding scheme, the electron bunches are dumped after each collision, and a new set of macroparticles with random Gaussian distribution is generated for each collision to simulate the electron bunch newly accelerated from the linac. The beams in storage rings can be either both the electron and positron beams in a ring-ring collider, or only the positron beam in a linac-ring collider.

After each collision, the bunch in a storage ring is transported linearly from the postcollision position to the rf cavity, where the effect of transverse damping and quantum excitation is simulated once a turn [13]. Each macroparticle is then linearly transported from the rf cavity to the precollision position. During each turn, the longitudinal position for a macroparticle relative to the beam center is changed along with its energy [13], as a result of the synchrotron oscillation together with the longitudinal damping and diffusion.

To obtain the initial distribution of the macroparticles for a bunch in a storage ring, we start by setting all the macroparticles at the center point of the bunch. Being transported through all the dynamics in the ring for several damping times in the absence of beam-beam interaction, the macroparticles eventually reach an equilibrium three-dimensional (3D) Gaussian distribution with specified nominal bunch sizes. Since no longitudinal motion is associated with the macroparticles for the electron bunch in the linac-ring collider, we distribute an equal number of macroparticles with transverse random Gaussian distribution to each slice in the bunch. The charges assigned to the macroparticles in different slices of the linac bunch are scaled to the parabolic longitudinal charge distribution.

III. A BENCHMARKING TEST

In Ref. [5], it is argued that the benchmarking of beam-beam simulation codes should use the physical phenomena predicted by theories and in the appropriate parametric regimes that have a clearly defined functional dependence. One of the proper candidates for this purpose of benchmarking is the coherent quadrupole beam-beam effect in ring-ring colliders. This phenomenon was predicted by Chao and Ruth [14], using a linearized Vlasov equation, and was first observed by Krishnagopal and Siemann in beam-beam simulation for the collision of round beams. It has the remarkable feature that, at tunes just below the quarter-integer, the beam distributions oscillate in an anticorrelated manner with period 2.

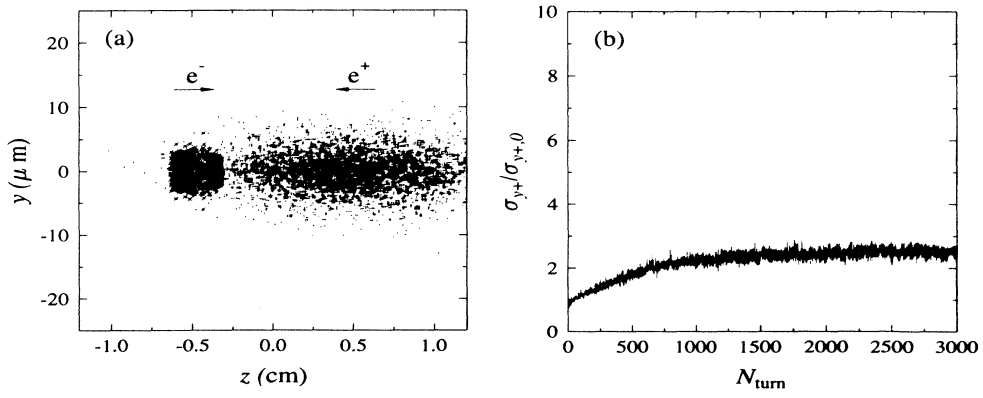

FIG. 4. Simulation results for (a) beam profiles before the 3000th collision and (b) verticle beam blowup factor vs number of turns. Here the number of macroparticles $N_{m-} = 1440$ is used for the electron bunch and $N_{m+} = 4000$ for the positron bunch.

TABLE I. Parameter list in simulation of coherent quadrupole effect as a benchmarking test.

Energy (E_0)	5.3 GeV
Revolution period (T_0)	2.56 μs
Transverse emittances ($\epsilon_x = \epsilon_y$)	1×10^7 m
Amplitude functions ($\beta_x^* = \beta_y^*$)	3 cm
Betatron tunes ($Q_x = Q_y$)	0.72
Damping decrement (δ)	1×10^{-3}
Current (I)	35 mA
Nominal beam-beam parameter (ξ_0)	0.121
Number of test particles	300

With the observation of the beam distribution oscillation with period 2 as the criterion for our benchmark test, we use the parameters shown in Table I [5] for our simulation. Here the two beams are round in the transverse plane and have no longitudinal length. The results of the functional dependence of the beam blowup factors and the luminosity vs the number of revolutions are shown in Figs. 5(a) and 5(b). The anticorrelated oscillation of beam sizes with period 2 is clearly demonstrated in Fig. 5(c). Figure 6 shows the corresponding variation of the transverse beam distributions, where each beam oscillates between the two modes of being dense and hollow in the core. These results agree well with the previous results [5,6,15,16] obtained using completely different simulation algorithms.

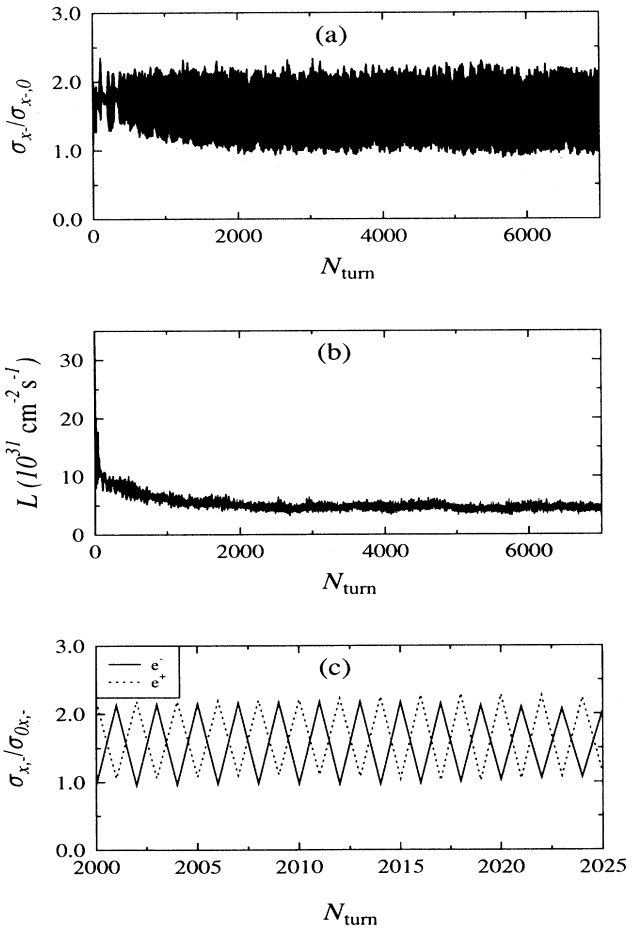

FIG. 5. Coherent quadrupole resonance in a ring-ring B factory for parameters in Table I. (a) Beam blowup factor for the e^- beam, (b) luminosity, and (c) beam blowup factors for the two beams vs number of turns.

IV. RESULTS FOR THE RING-RING BEAM-BEAM EFFECTS

Another test of our code is the simulation of the beam-beam effect in the ring-ring B factory. For this study we use the parameters in the PEP B factory proposal [7], as shown in Table II. The nominal luminosity is $\mathcal{L}_0 = 3 \times 10^{33}\ \mathrm{cm}^{-2}\mathrm{s}^{-1}$, and the four nominal beam-beam tune shift parameters are all set to be $\xi_0 = 0.03$. Here each bunch, divided into five slices, is represented by 300 macroparticles. The macroparticles themselves are Gaussian charge distributions with sizes half the nominal bunch sizes.

The beam-beam results in Ref. [7] are obtained at the working point $(\nu_x, \nu_y) = (0.9, 0.5)$ for both beams. However, at this working point, we observed a much bigger blowup for the e^+ beam than that shown in Ref. [7]. It is noticed that the parameters for the e^+ beam are close to the relation $\nu_s = \nu_x - \nu_y$. Hence, for the following simulation, the fractional tunes for both beams are selected at $(\nu_x, \nu_y) = (0.9, 0.6)$ to avoid the resonance.

In Fig. 7, we show the initial distribution of centers of the macroparticles for the two colliding beams. The numbers of the macroparticles in each slice are shown in Fig. 8. The dynamics for both beams is simulated over three damping times. The behavior of $\sigma_{y+}/\sigma_{y+,0}$ is shown in Fig. 9(a), and the behavior of the luminosity can be seen in Fig. 9(b). It turns out that as the result of beam-beam interaction, the bunch sizes increase in the first damping time and consequently cause the decrease of the luminosity. A set of equilibrium values can be reached for all the bunch sizes in a period of several damping times, from which the dynamical beam-beam tune-shift parameters can be evaluated using Eq. (1.2).

TABLE II. Ring-ring B factory parameter list.

	e^+	e^-
E (GeV)	3.1	9
s_B (m)	1.26	1.26
f_c (MHz)	476.0	476.0
α	1.15×10^{-3}	2.41×1^{-3}
ν_s	0.0403	0.0520
σ_l (cm)	1	1
N_b	5.61×10^{10}	3.88×10^{10}
ϵ_{0x} (nm rad)	92	46
ϵ_{0y} (nm rad)	3.6	1.8
β_x^* (cm)	37.5	75.0
β_y^* (cm)	1.5	3.0
σ_{0x}^* (μm)	186	186
σ_{0y}^* (μm)	7.4	7.4
τ_x (turns)	4400	5014
τ_y (turns)	4400	5014

The nominal beam-beam tune-shift parameter ξ_0 can be changed by varying the charges in the two beams simultaneously. In Fig. 10 we show the equilibrium bunch sizes, luminosity, and dynamical beam-beam tune-shift parameters as functions of ξ_0. One finds that the luminosity plot in Fig. 10(b) is quantitatively comparable with Fig. 4-88 in Ref. [7]. The saturation of the dynamical ξ_{y+} to a value of $\xi_{\rm lim} \approx 0.04$ is shown in Fig. 10(c).

The significant phenomenon one observes is the blowup of the vertical size for the low-energy beam, which qualitatively agrees with the results in Ref. [7]. This limiting effect on the beam in the low-energy ring is unfavorable for further asymmetrization of the energies in the two rings.

V. RESULTS FOR THE LINAC-RING BEAM-BEAM EFFECTS

We now focus our attention on the simulation of the beam-beam effect in the linac-ring B factory. There have been several parameter lists proposed for the design of this colliding scheme [1–3]. The one shown in Table III is used here for our simulation. Notice that the proposed nominal luminosity is $\mathcal{L}_0 = 1 \times 10^{34}$ cm^{-2}s^{-1}, and the nominal beam-beam parameters are $\xi_{y+,0} = 0.056$ and $D_{y-,0} = 273.7$, indicating strong beam-beam interaction.

TABLE III. Linac-ring B factory parameter list.

Linac (e^-)	Storage ring (e^+)
$E_- = 3.5$ GeV	$E_+ = 8.0$ GeV
$N_- = 0.544 \times 10^9$	$N_+ = 6.1 \times 10^{11}$
$f_c = 20.0$ MHz	$n_B = 30$
$\epsilon_{x-,0} = 5.75$ nm	$\epsilon_{x+,0} = 5.75$ nm
$\epsilon_{y-,0} = 0.37$ nm	$\epsilon_{y+,0} = 0.057$ nm
$\beta^*_{x-,0} = 3.32$ mm	$\beta^*_{x+,0} = 3.33$ mm
$\beta^*_{y-,0} = 3.33$ mm	$\beta^*_{y+,0} = 21.55$ mm
$\sigma^*_{x-,0} = 4.37$ μm	$\sigma^*_{x+,0} = 4.37$ μm
$\sigma^*_{y-,0} = 1.11$ μm	$\sigma^*_{x+,0} = 1.11$ μm
$\sigma_{z-} = 2.64$ mm	$\sigma_{z+} = 3.3$ mm
$D_{x-,0} = 69.6$	$\nu_s = 0.07$
$D_{y-,0} = 273.7$	$\tau_x = 0.9$ msec
	$\tau_y = 2.4$ msec
	$\tau_\delta = 6.9$ msec
	$\xi_{x+,0} = 0.002$
	$\xi_{y+,0} = 0.056$
$\mathcal{L}_0 = 1.1 \times 10^{34}$ cm^{-2}sec^{-1}	

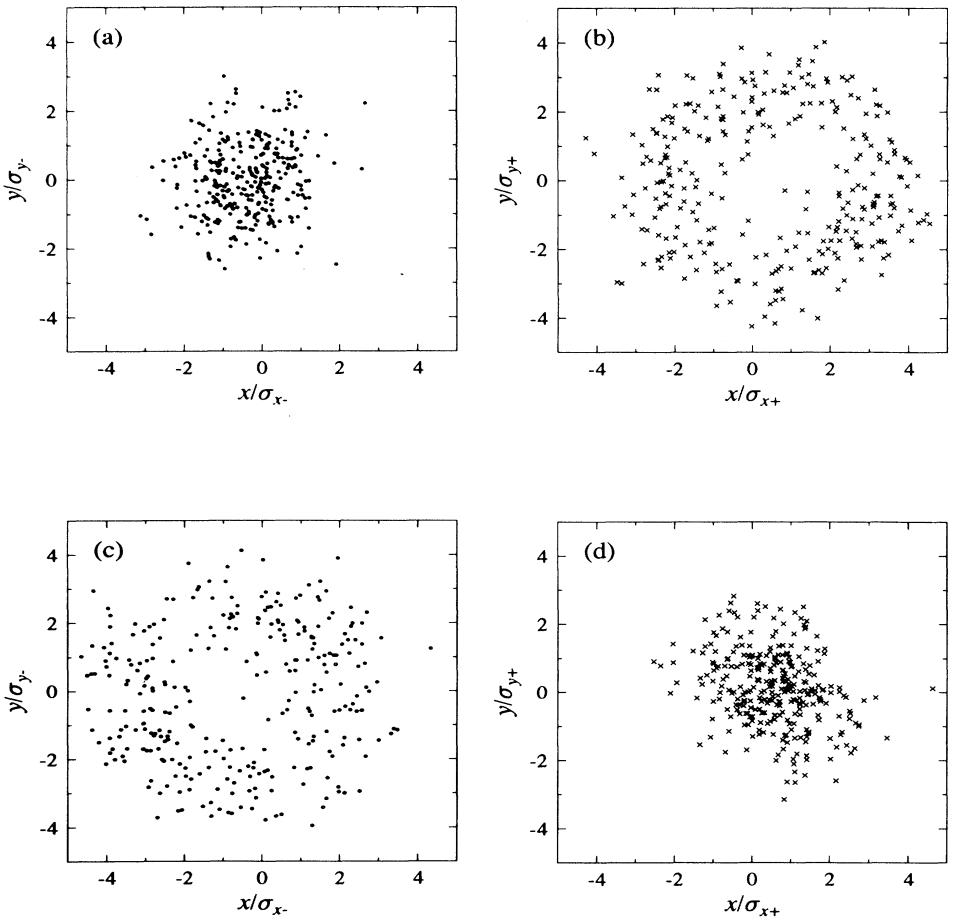

FIG. 6. Transverse distribution of electron and positron bunches. (a) Electron macroparticles at 2000th turn; (b) positron macroparticles at 2000th turn; (c) electron macroparticles at 2001th turn; and (d) positron macroparticles at 2001th turn.

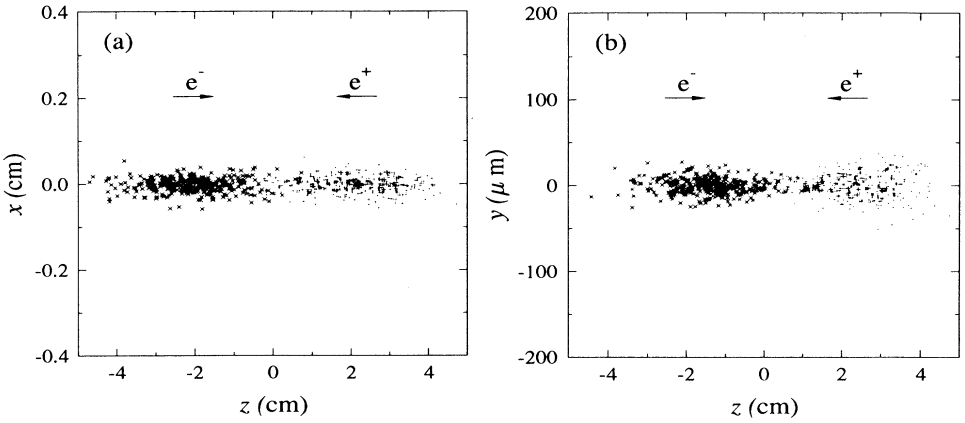

FIG. 7. Beam profiles in the (a) X-Z plane and (b) Y-Z plane before the first collision for a ring-ring collider using parameters in Ref. [7].

Our goal is to study the beam-beam tune-shift limit for the linac-ring collider, and to observe the dominant dynamics responsible for the beam-beam limitation. The simulation-related parameters are listed in Table IV.

The profiles of the two beams in the Y-Z plane before and after the first collision are shown in Fig. 11. For the e^- beam, the numbers of macroparticles are evenly distributed among the slices, with the longitudinal parabolic charge distribution characterized by the difference in the charges carried by macroparticles in different slices. This is shown in Fig. 12(a). The longitudinal Gaussian charge distribution for the e^+ beam is simulated by the longitudinal Gaussian distribution of macroparticles carrying the same amount of positive charges, as shown in Fig. 12(b). In the simulation, the e^+ beam is circulated in the storage ring, experiencing a beam-beam collision at IP once a turn with a new electron bunch, and also undergoes the ring dynamics including the linear betatron oscillations, synchrotron oscillations, as well as the damping and diffusion in all three dimensions. The evolution of the positron vertical bunch size and the luminosity of beam-beam collisions in about three damping times of the vertical motion are shown in Fig. 13, which demonstrates that the luminosity reaches an equilibrium value lower than the nominal one as the result of beam blowup.

To understand the cause of the beam blowup in the linac-ring beam-beam simulation, the trace of certain e^- macroparticles and also the variation of rms size for each e^- slice through the e^+ bunches during the first collision are plotted in Fig. 14. The formation of pinches when the e^- macroparticles oscillate through the e^+ bunch is clearly seen as the effect of the high disruption of the e^- bunches (here $D_{ey} = 273.7$). It is expected that the consequent deep modulation of the e^- envelope in the collision processes will have a significant impact on the stability of the positron bunches by inducing (1) strong nonlinearity at the pinch points and (2) strong synchro-

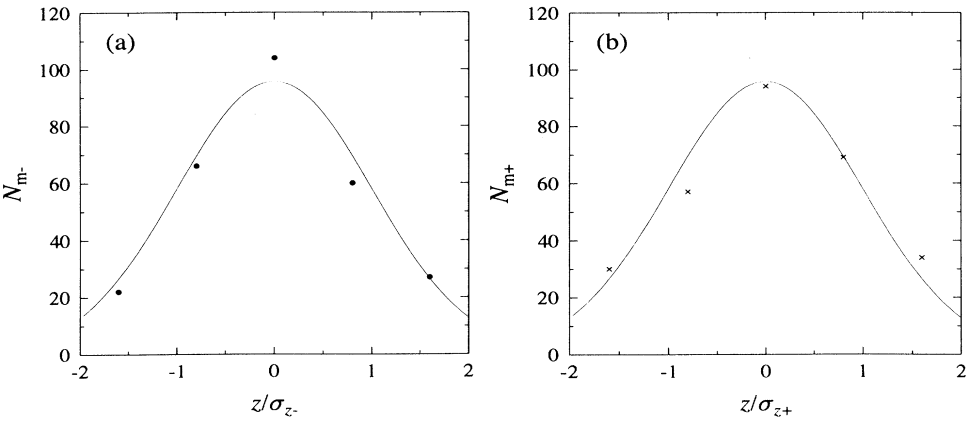

FIG. 8. Initial numbers of macroparticles for the five slices in e^- and e^+ bunches, respectively, which are compared with the ideal Gaussian distribution (solid curves).

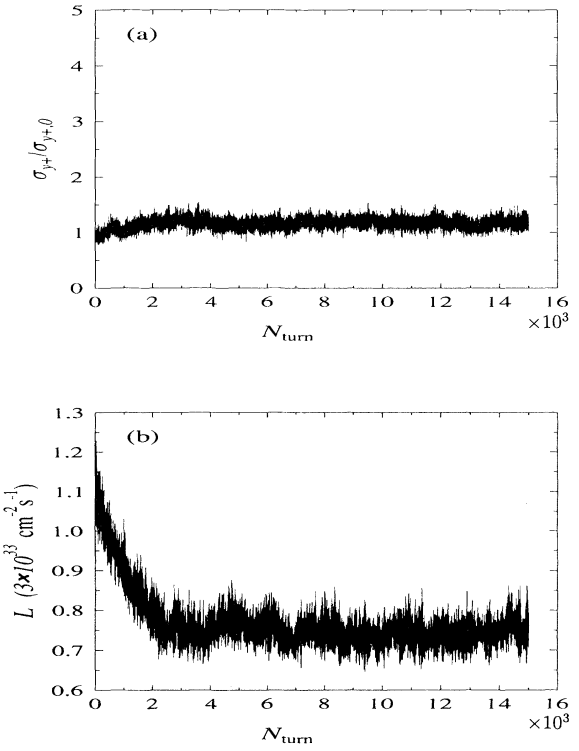

FIG. 9. Results of (a) vertical beam blowup factor for the e^+ beam and (b) luminosity for parameters in Table II.

betatron coupling. This is believed to be the major mechanism for the observed beam blowup in Fig. 13(a).

As pointed out by S. Heifets [3], the effect of the pinching of the electron beam on the stability of positrons can be minimized by the proper choice of initial conditions for the electron beam entering the interaction region. The underlying idea is that with a large transverse momentum spread in the phase space for the incoming electrons, the focusing points of the electrons due to their strong interaction with the positron beam are spread out longitudinally, thereby producing a much smoother envelope distribution for the e^- bunch. This scheme is called matching, meaning that the initial condition of the electron beam is chosen such that the two colliding beams are matched in sizes at IP, i.e., $\sigma^*_{x-,0} = \sigma^*_{x+,0}$ and $\sigma^*_{y-,0} = \sigma^*_{y+,0}$, when the beam-beam focusing is included. In the practical design, the effect of matching can be provided by the hourglass effect due to the strong focusing of the e^- beam at IR. From simulations using several parameter sets [17], it is found that at high disruption ($D_{ey} \approx 300$), matching occurs when $\beta^*_{y-} \approx 0.5\sigma_{z+}$, in contrast to the usual requirement $\beta^*_{y-} \approx \sigma_{z+}$. Thus, although matching requires somewhat stronger focusing, it is not beyond practical considerations.

TABLE IV. Parameters for simulation.

	e^-	e^+
Number of slices	9	45
Number of macros	360	1000
Aspect ratio of macros	3.93	
Sizes of macros	0.5 × (beam sizes)	

For the parameters in Table III, where $\beta^*_{y-} \approx \sigma_{z+,0}$, the hourglass effect is not significant enough to provide a natural matching. Hence, a stronger focusing of the e^- bunch prior to the IR is simulated by determining the initial condition for the e^- bunch through tracking the matched e^- bunch at IP back to the beginning of the interaction. Compared with Fig. 14 for the nonmatching case, a smoother envelope distribution of the e^- bunch for the matching case is shown in Fig. 15. Similar to Fig. 13, the long term behavior of the positron bunch size and the luminosity can also be obtained in the case of matching.

We then proceed to study the beam-beam effect for both matching and nonmatching cases by varying $\xi_{y+,0}$ while fixing $D_{y-,0}$. This is done by varying the total charge of the e^- beam N_- while fixing the total charge of the e^+ beam N_+. The dependence of the equilibrium values of the beam blowup factor and luminosity with respect to different $\xi_{y+,0}$ is shown in Fig. 16. As shown in Fig. 16(a), for the nonmatching case, the beam starts to

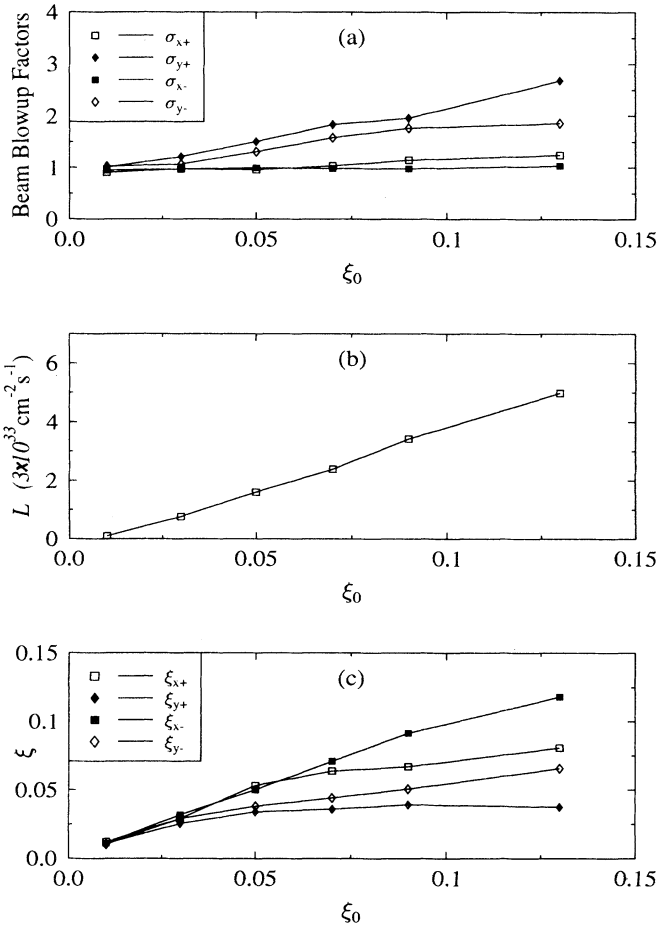

FIG. 10. Results of beam-beam effect for ring-ring B factory parameters: (a) Beam blowup factors, (b) luminosity, and (c) dynamical ξ vs ξ_0.

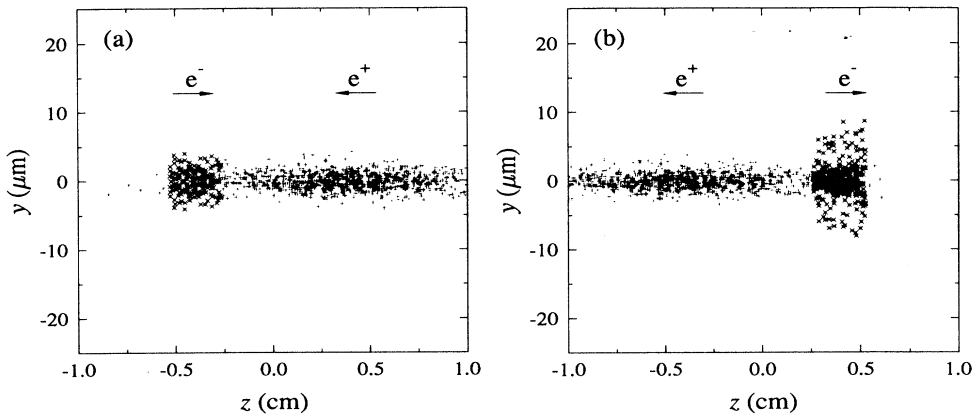

FIG. 11. Beam profiles in the Y-Z plane (a) before and (b) after the first collision with beam parameters shown in Table III.

blow up around $\xi_{y+,0} = 0.02$, whereas the blowup takes place around $\xi_{y+,0} = 0.05$ if matching applies. Also the extent of beam blowup as $\xi_{y+,0}$ increases for the nonmatching case is much larger than the matching situation. In Fig. 16(b), the luminosities deviate from the nominal (no beam-beam interaction) behavior as the result of beam blowup [here the luminosity and the beam sizes do not straightforwardly satisfy Eq. (1.1) because of the focusing phenomena involved for the e^- macroparticles]. It is shown that, for $\xi_{y+,0}$ above the value of 0.06, the luminosity in the matching case increases slowly with values larger than the saturated value in the nonmatching cases. The above comparison of the beam-beam effect with and without matching manifests the effect of envelope modulation of the e^- bunches.

The results in Figs. 13 and 16 were obtained for the fractional betatron tune (Q_{x+}, Q_{y+}) being $(0.64, 0.54)$. As the further investigation of the beam-beam effect in linac-ring scenarios, we studied the dependence of the equilibrium beam blowup factor $\sigma_{y+}/\sigma_{y+,0}$ on the choice of (Q_{x+}, Q_{y+}) for the storage ring beam. Since the simulation is strong-strong and time consuming, the blowup is computed on sporadic points in the tune plane that are reasonably chosen in interesting areas instead of sweeping the grids in the tune plane. The following are the descriptions of the general behavior observed. First, for the low-disruption cases ($D_{y-,0} < 1$), one can see clearly the transverse resonance structure and the synchrotron sidebands in the tune plane. This is similar to the beam-beam interaction in the ring-ring collider, when the collisions of the two beams take place without the oscillation of the electrons or pinching of the electron beam. Secondly, when matching is applied to the high-disruption case ($D_{y-,0} = 273.3$), the transverse resonance structure can be observed as a strong localized enhancement of the low-level beam blowup in the tune plane. This indicates that when matching applies, apart from the residual modulation of the e^- envelope, the beam-beam limit is approximately caused by the same nonlinearity effect as in the ring-ring situation. Lastly, for the high-disruption case without matching, the general phenomenon found is that when the modulation of σ_{y-} becomes deeper as $D_{y-,0}$ increases, the equilibrium bunch size σ_{y+} varies from the unperturbed value in most of the tune plane to the situation of overall blowup. This agrees with the results obtained by Gerasimov [18] using a weak-strong

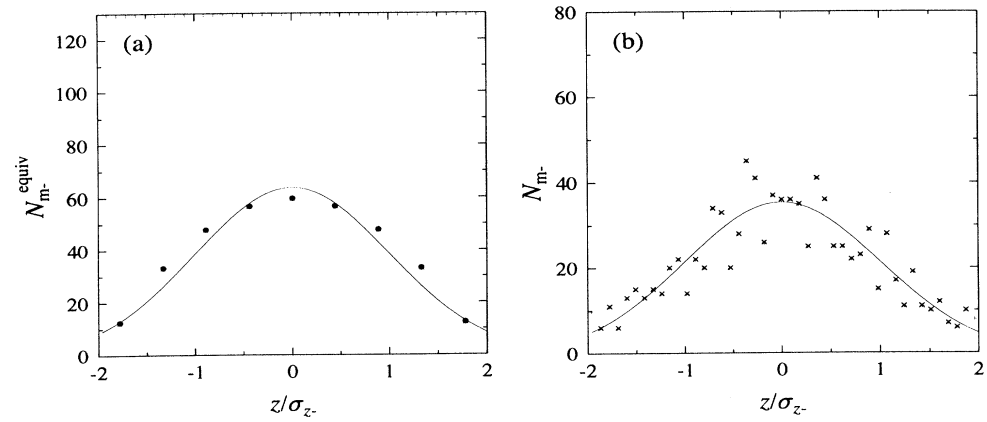

FIG. 12. (a) Equivalent number of macros in each slice for the e^- beam; and (b) number of macroparticles in each slice for the e^+ beam.

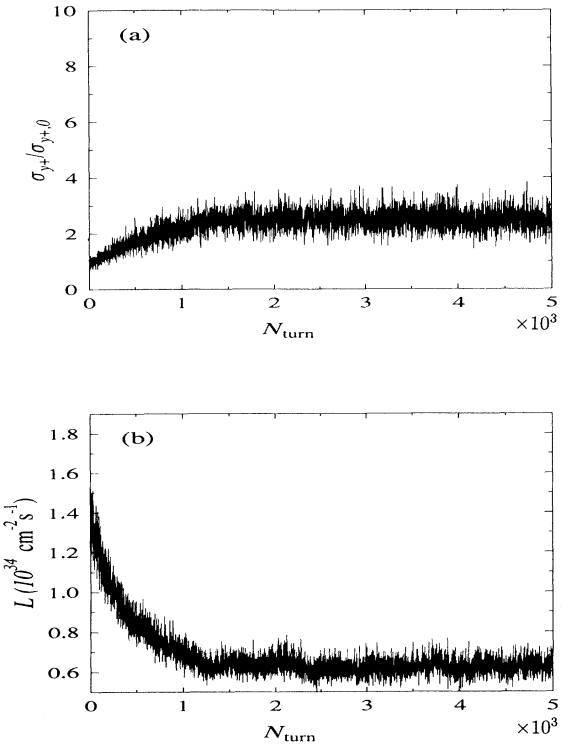

FIG. 13. Results of (a) beam blowup for the positron beam and (b) luminosity during 5000 turns for parameters in Table III.

simulation with envelope-modulated electron bunches. It is also found that when the synchrotron motion of the e^+ beam is turned off in the simulation, the equilibrium beam blowup factor is much smaller compared to that obtained in the presence of the synchrotron motion. This implies that the overall beam blowup in the tune plane is mainly caused by the synchrobetatron coupling induced by the envelope modulation of the e^- beam.

It is important to ensure the numerical stability of the simulation results with respect to the simulation parameters. As shown in Figs. 3 and 4, the same equilibrium beam blowup value is obtained for different numbers of macroparticles for the simulation. We also found that the results agree for different numbers of slices for the two beams (5 for the e^- bunch and 25 for the e^+ bunch, as opposed to our previous parameters—9 for the e^- bunch and 45 for the e^+ bunch). With all these checks, we conclude that the stability of the positron bunch is strongly affected by the pinching of the e^- bunch in the nonmatching case; on the other hand, the beam-beam tune-shift limit for the e^+ bunch can be made comparable with that in the ring-ring beam-beam interaction, provided that proper initial condition is set for the e^- bunches.

VI. EFFECT OF JITTERS

Since the number of macroparticles is limited in the simulation, a fluctuation of the transverse offset for each slice in the two beams is inevitable. These offsets are random and of the order $\sigma_{x,y}^{\mathrm{slice}}/\sqrt{N_m^{\mathrm{slice}}}$, where $\sigma_{x,y}^{\mathrm{slice}}$ are the rms sizes of a given slice simulated by N_m^{slice} number of macroparticles. Without any treatment of these offsets in the simulation, the positron bunch shows a kink instability in the absence of synchrotron oscillations. It has been observed [19] that as the highly disrupted electron particles oscillate through the positron bunch, the effects of the offsets in the previous positron slices are passed to the later slices by the electrons. After many turns, the offsets in the positron slices are cumulatively enhanced in a coherent manner by this dipole interaction. Further simulation shows that the coherence in the dipole motion tends to be suppressed by synchrotron motion of the positron particles. The results of the beam-beam effect in a linac-ring collider presented in the previous section are obtained by removing the offset effects in the force calculation of the simulation, corresponding to ideal head-on collisions.

In reality, however, the e^- bunches from the linac could fluctuate in intensity, transverse position, longitudinal

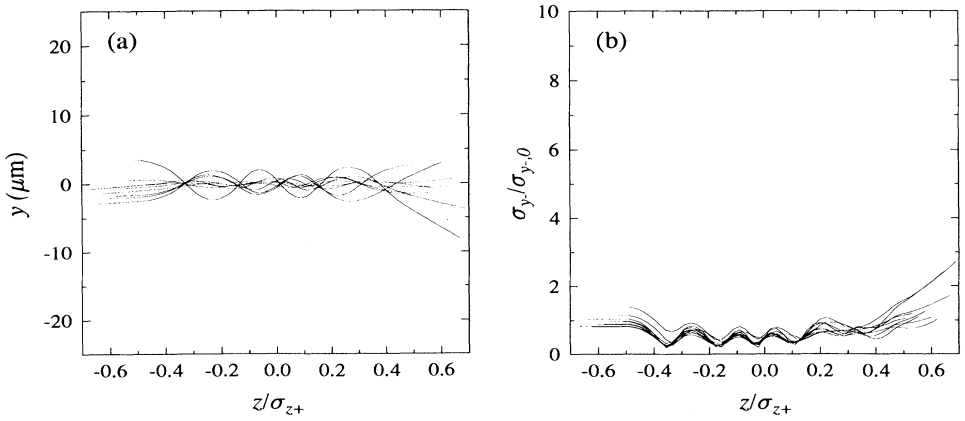

FIG. 14. Plots of (a) traces of e^- macroparticles and (b) variations of rms size for e^- slices in the Y-Z plane in the rest frame of the e^+ bunch *without* matching.

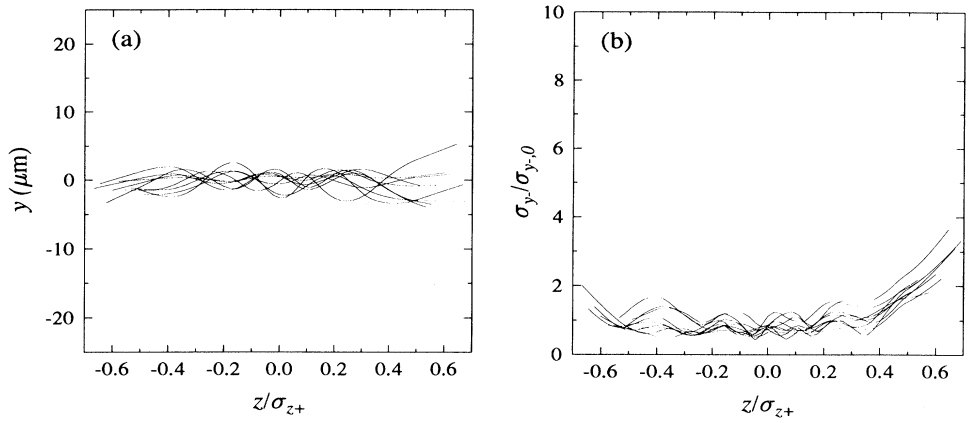

FIG. 15. Plots of (a) traces of e^- macroparticles and (b) variations of rms size for e^- slices in the Y-Z plane in the rest frame of the e^+ bunch *with* matching.

position (timing), and possibly shape. It is important to investigate the impact of these possible jitters of the linac beam on the stability of the storage-ring beam. A complete description of the problem includes the coherent motion of the two beams, the effect of external colored noise on the nonlinear dynamical system, and the multidimensional couplings as well as the effect of damping and quantum diffusion.

In Ref. [20], the first-order effects of white noise jitters are estimated analytically by using a one-dimensional linear model. It shows that the required jitter tolerances are at the margin of the precision of measurements. Weak-strong simulations without damping [21] basically confirmed the above analytical prediction. As suggested in Ref. [21], the weak-strong simulation reveals the *initial* emittance growth of the e^+ beam. In the long term, the blowup of the e^+ beam will reduce the disruption of the e^- beam, and thus the effects of the pinches.

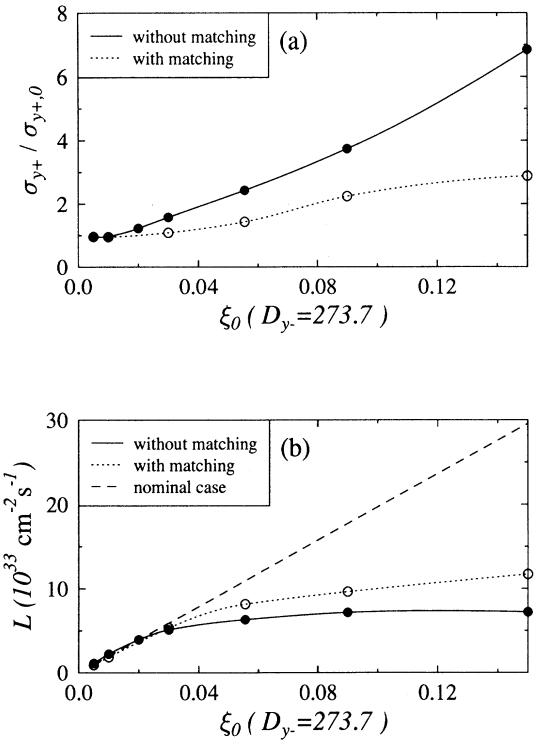

FIG. 16. Results of beam-beam effect for a linac-ring B factory using parameters in Table III. (a) Beam blowup factor and (b) luminosity vs nominal tune shift. Here ξ_0 is changed by varying N_- only.

Here we studied the effect of the intensity jitter in order to reach an understanding consistent with previous predictions. First, a weak-strong simulation was carried out using an analytic beam-beam force formula for round beams, with the round positron beam represented by 500 particles. For the calculation, the damping times used were $\tau_x = \tau_y = 2.4$ ms, and the jitter of the electron current was 10%. The beam-beam tune-shift parameters were set at $\xi_{x+,0} = \xi_{y+,0} = 0.055$, and the beams were assumed to have no longitudinal lengths. The fractional betatron tunes were chosen to avoid the linear weak-strong instability [22]. The destructive effect of intensity jitter, when the force is *linear*, is shown in Fig. 17(a). Figure 17(b) shows that the presence of damping can slow down the rate of beam blowup, but the beam is still far from stability. This is because the magnitude of the intensity jitter here is above the stability threshold predicted in Ref. [20] based on the linear model. However, when the *nonlinear* beam-beam force is used at IP, as shown in Fig. 18(a), the intensity jitter is much less destructive than that in a *linear* case. Furthermore, when transverse damping is applied to the *nonlinear* beam-beam interaction, the stability of the e^+ beam is restored, as shown in Fig. 18(b) (the same result was obtained by Johnson [23]). The result in Fig. 18(a) is consistent with the results in Ref. [21], where the amplitude growth of positron particles is studied in a weak-strong simulation with synchrotron motion included. However, the effect of synchrobetatron coupling is small when studying particles with small synchrotron amplitudes [23].

We next studied the effect of jitters using our strong-strong beam-beam simulation, using the machine parameters in Table III and simulation parameters in Table IV.

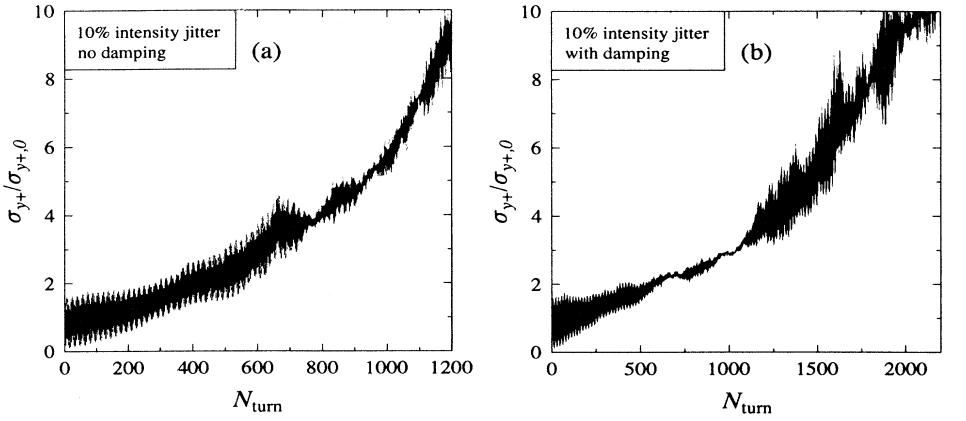

FIG. 17. Vertical beam blowup for a round positron beam simulated by 500 particles. Here the analytic *linear* beam-beam transverse forces with $\xi_{x+,0} = \xi_{y+,0} = 0.055$ are used at IP for weak-strong simulation. The beam is assumed to have no longitudinal length.

In the absence of the synchrotron motion, the same feature of the effect of damping in a nonlinear potential as shown in Fig. 18 is observed. We thus conclude that the internal jitter caused by the shot noise in the simulation plays a negligible role in the study of the effect of the external intensity jitter. With the inclusion of the synchrotron motion, however, the e^+ beam blows up even when the linac beam has no intensity jitters, as shown in Fig. 19(a). This is the result of the synchrobetatron coupling induced by the deep envelope modulation of the e^- beam. It is shown in Fig. 19(b) that the presence of jitter gives only a 10% increase in the beam blowup compared to the case in Fig. 19(a). Moreover, when damping is applied, the effect of jitter can hardly be seen when we compare the result in Fig. 19(c) with that in Fig. 13(a). The latter is obtained in the absence of jitter.

In the above study, we used random white noise for the intensity jitter. In the actual experiment, the power spectrum for the jitters of the linac beam depends on the characteristics of the photo cathode gun. For example, in a few-millisecond circulation time for the e^+ beam, 60-Hz noise acts as a constant offset; the e^+ beam would be more responsive to noise with frequencies in the kilohertz range. To study the effect of jitters of the linac beam for a specific design, it is important to know the power spectrum of the jitter and to take the complete dynamics for the e^+ beam into account.

VII. SUMMARY

In this study, a strong-strong beam-beam simulation is developed based on a macroparticle model. The motion of the macroparticles is 3D, and the effects of damping and quantum diffusion in the storage ring are also included. The dependence of the computation results on the simulation parameters, such as the size and the number of the macroparticles chosen, is also estimated. As a benchmarking test, this simulation reveals the same coherent quadrupole effect in the ring-ring collider as observed by others.

This simulation scheme is first applied to study the beam-beam effect in a ring-ring B factory, using the parameters in the PEP B factory proposal. The beam-beam results thus obtained agree qualitatively with the published results. Quantitative comparison of the results

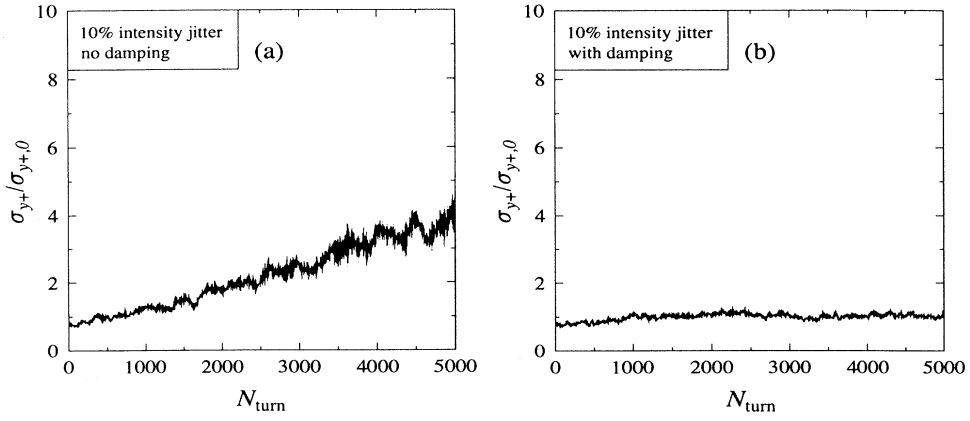

FIG. 18. Vertical beam blowup for a round positron beam simulated by 500 particles. Here the analytic *nonlinear* beam-beam transverse forces with $\xi_{x+,0} = \xi_{y+,0} = 0.055$ are used at IP for weak-strong simulation. The beam is assumed to have no longitudinal length.

requires further knowledge of the details of the simulations involved. We then use our simulation to study the beam-beam effect in a linac-ring B factory. For $D_{y-,0} = 273.7$, the e^+ beam starts to blow up in the vertical direction at $\xi_{y+,0} = 0.02$. On the other hand, if the precollision state of the e^- bunches is properly chosen to smooth out the pinches, the beam-beam tune-shift limit for the e^+ beam is found to be around 0.05, which is comparable with that value in a ring-ring B factory.

The effect of intensity jitter in the linac beam on the stability of the storage-ring beam is also tested using our strong-strong simulation. With the inclusion of all the possible dynamics in the simulation, the extremely unstable situation for the positron bunch predicted by the weak-strong simulation without damping and an analytic model based on the linear beam-beam interaction is not observed.

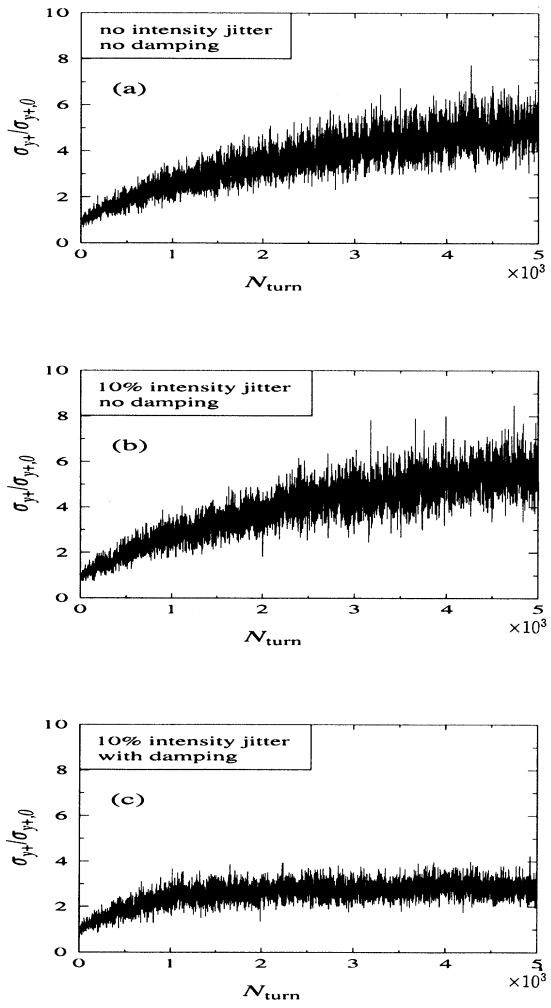

FIG. 19. Vertical beam blowup in the strong-strong simulation, with parameters in Table III. Here the synchrotron motion is included.

ACKNOWLEDGMENTS

We have benefited greatly from conversations with G. A. Krafft on the macroparticle model for the beam-beam interaction, and from the original code SWARM written by J. Boyce. The information provided by C. D. Johnson, S. Krishnagopal, and M. A. Furman is gratefully acknowledged. The discussion with H. Liu on the screening effect of the macroparticle model was also illuminating. This work is supported by U.S. DOE Contract No. DE-AC05-84ER40150.

APPENDIX

To estimate the effect of the finiteness of (1) the sizes of macroparticles and (2) the number of macroparticles in each bunch on the results of the beam-beam interaction using the macroparticle model, we take the familiar *Gaussian* bunch distribution as an example.

First we study the effect of finite size of the macroparticles. Consider a system of macroparticles. Let $\rho_c(\mathbf{x},t)$ denote the distribution function for the center of the macroparticles. And let $S(\mathbf{x})$ denote the charge distribution in each single macroparticle, which corresponds to its finite size. The overall charge distribution function of the system, $\rho(\mathbf{x},t)$, is then [24]

$$\rho(\mathbf{x},t) = \int d\mathbf{x}' S(\mathbf{x}-\mathbf{x}')\rho_c(\mathbf{x}',t). \tag{A1}$$

The Fourier transform of the above equation gives

$$\tilde{\rho}(\mathbf{k},t) = \tilde{S}(\mathbf{k})\tilde{\rho}_c(\mathbf{k},t), \tag{A2}$$

where

$$\tilde{S}(\mathbf{k}) = \int d\mathbf{x} S(\mathbf{x}) e^{-i\mathbf{k}\mathbf{x}}, \tag{A3}$$

and $\tilde{\rho}_c(\mathbf{k},t)$ and $\tilde{\rho}(\mathbf{k},t)$ are transformed from $\rho_c(\mathbf{x},t)$ and $\rho(\mathbf{x},t)$ in a similar way, respectively.

Assume that a slice of a charged beam is represented by N_m macroparticles. The centers of the macroparticles are subject to a *continuous* 2D Gaussian distribution with the rms bunch sizes σ_{xB} and σ_{yB}, namely,

$$\rho_c(x,y) = \frac{N_m}{2\pi\sigma_{xB}\sigma_{yB}} e^{-\frac{x^2}{2\sigma_{xB}^2}-\frac{y^2}{2\sigma_{yB}^2}},$$

or (A4)

$$\tilde{\rho}_c(k_x,k_y) = N_m e^{-\frac{k_x^2\sigma_{xB}^2}{2}-\frac{k_y^2\sigma_{yB}^2}{2}}.$$

Let each macroparticle be a 2D Gaussian charge distribution carrying a charge q_m, with rms sizes σ_{xm} and σ_{ym},

$$S(x,y) = \frac{q_m}{2\pi\sigma_{xm}\sigma_{ym}} e^{-\frac{x^2}{2\sigma_{xm}^2} - \frac{y^2}{2\sigma_{ym}^2}},$$

or (A5)

$$\tilde{S}(k_x,k_y) = q_m e^{-\frac{k_x^2\sigma_{xm}^2}{2} - \frac{k_y^2\sigma_{ym}^2}{2}}.$$

As the result of Eq. (A2), the system of macroparticles yields an overall Gaussian distribution, which satisfies

$$\tilde{\rho}(k_x,k_y) = N_m q_m e^{-\frac{k_x^2(\sigma_{xB}^{\rm eff})^2}{2} - \frac{k_y^2(\sigma_{yB}^{\rm eff})^2}{2}}. \quad \text{(A6)}$$

Here $\sigma_{xB}^{\rm eff}$ and $\sigma_{yB}^{\rm eff}$ are the effective rms bunch sizes,

$$\sigma_{xB}^{\rm eff} = \sqrt{\sigma_{xB}^2 + \sigma_{xm}^2} \quad \text{and} \quad \sigma_{yB}^{\rm eff} = \sqrt{\sigma_{yB}^2 + \sigma_{ym}^2}. \quad \text{(A7)}$$

We thus conclude that a system of continuously Gaussian distributed macroparticles, with the inner charge distribution for each macroparticle being also Gaussian, is equivalent to a Gaussian distribution of point particles with the rms sizes given by Eq. (A7). As a consequence, the force generated by a distribution of charged *macroparticles* deviates from that generated by the same distribution of *point* charges. As shown in Fig. 2, this deviation is most obvious at the standard deviation of the distribution. This is called the edge effect. Also the luminosity for two overlapping slices in two colliding beams, which are simulated by macroparticles, satisfies Eq. (1.1), with the bunch sizes replaced by the effective bunch sizes given by Eq. (A7). If the sizes for the macroparticles are properly chosen to satisfy

$$(\sigma_{xm}/\sigma_{xB})^2 \ll 1 \quad \text{and} \quad (\sigma_{ym}/\sigma_{yB})^2 \ll 1, \quad \text{(A8)}$$

the effects of finite size of macroparticle on the bias of the calculated results are negligible.

Next we discuss the effect of the finiteness of the number of macroparticles. For a system of a finite number of macroparticles, $\rho_c(\mathbf{x},t)$, the distribution function for the center of the macroparticles will contain high-frequency components instead of behaving smoothly, as in Eq. (A4). Since each macroparticle is a Gaussian distribution given by Eq. (A5), we have $\tilde{S}(k_x,k_y) \ll 1$ for $k_x \gg 1/\sigma_{xm}$ and $k_y \gg 1/\sigma_{ym}$. As a result, the high-frequency component in the overall charge distribution $\rho(x,y)$ is suppressed according to Eq. (A2). This is the screening effect of the finite size of the macroparticles. We define N_0 as

$$N_0 = \frac{\sigma_{xB}\sigma_{yB}}{\sigma_{xm}\sigma_{ym}}, \quad \text{(A9)}$$

which is the number of macroparticles required to cover the bunch without overlapping. It can be shown that under the conditions of Eq. (A8), the relative fluctuation of the luminosity $\mathcal{L}$ for the interaction of the bunch with other charge distributions is small when the number of macroparticles in the bunch satisfies $N_m/N_0 \gg 1$, namely [25],

$$\langle\Delta\mathcal{L}^2\rangle/\langle\mathcal{L}\rangle^2 \ll 1 \quad \text{when} \quad N_m/N_0 \gg 1. \quad \text{(A10)}$$

Here the ratio N_m/N_0 characterizes the degree of overlapping of the macroparticles.

Given the number of macroparticles in each bunch, the collisional effect due to the discreteness of the distribution can be suppressed by assigning finite sizes to the macroparticles. However, it is inevitable to have a residual low-frequency fluctuation in the overall charge distribution due to the finiteness of the number of macroparticles. In our simulations, since the number of macroparticles is limited strongly by the computer time, we choose the sizes of the macroparticles to be relatively large (for most of our computations, we choose $\sigma_{xm}/\sigma_{xB} = 0.5$ or $\sigma_{xm}/\sigma_{xB} = 0.5$; smaller macroparticle sizes were used occasionally for error estimation) in order to have a better screening from the collisional effect. As the rms sizes of each slice in a bunch are updated for each step of advance in a collision, the sizes of the macroparticles in the slice are varied accordingly.

It should be noted that the aspect ratio of the macroparticles $R_m = \sigma_{xm}/\sigma_{ym}$ is fixed through the lookup table for the beam-beam forces. On the other hand, for interactions involving the pinch or blowup of the beams, the aspect ratio for each slice of a bunch $R_B = \sigma_{Bx}/\sigma_{By}$ evolves with time. Special care should be taken to ensure that Eq. (A8) is always satisfied. In the simulation, the size of the macroparticles was chosen to be proportional to the size of the corresponding slice in the bunch, with the proportionality parameter $r(r^2 \ll 1)$. When $R_B < R_m$, we set $\sigma_{mx} = r\sigma_{Bx}$, which gives $\sigma_{my} = r(R_B/R_m)\sigma_{By}$. In contrast, when $R_B > R_m$, we set $\sigma_{my} = r\sigma_{By}$, which leads to $\sigma_{mx} = r(R_m/R_B)\sigma_{Bx}$.

A reasonable extension of the above results to the simulation of the interaction for beams with *general* charge distribution is that the size of the macroparticles should be small compared to the characteristic length of the overall charge distribution, and the number of macroparticles should be enough so that the macroparticles overlap one another to cover the dense region of the distribution.

[1] P. Grosse-Wiesmann, Stanford Linear Accelerator Center Report No. SLAC-PUB-4545, 1988 (unpublished).
[2] J. Bisognano *et al.* (unpublished).
[3] S. A. Heifets, G. A. Krafft, and M. Fripp, Nuclear Instrum. Methods Phys. Res. A **295**, 286, (1990).
[4] J. R. Boyce, S. Heifets, and G. A. Krafft (unpublished).
[5] S. Krishnagopal and R. H. Siemann, Lawrence Berkeley Laboratory Report No. LBL-32581, 1992 (unpublished).
[6] S. Krishnagopal (private communication).
[7] Stanford Linear Accelerator Center Report No. SLAC-PUB-372, 1991 (unpublished).
[8] Y. Chin, DESY Report No. DESY 87-011, 1987 (unpub-

lished).
[9] M. A. Furman (private communication).
[10] Private communication with G. A. Krafft. The macroparticle model used here was originally developed to study the beam-beam interaction for round beams by G. A. Krafft and J. S. Wurtele based on R. Sah's SMASH program. In the present simulation the model is generalized by using Gaussian macroparticles of any given aspect ratio to study the interaction of elliptical beams.
[11] G. A. Krafft, CEBAF Report No. CEBAF TN-92-032, 1992 (unpublished).
[12] M. Bassetti and G. A. Erskine, CERN Report No. CERN-ISR-TH/80-06, 1980 (unpublished).
[13] S. Krishnagopal and R. H. Siemann, Cornell Internal Note No. CBN/88-1, 1988 (unpublished).
[14] A. W. Chao and R. D. Ruth, Part. Accel. **16**, 201, (1985).
[15] S. Krishnagopal and R. H. Siemann, Cornell Internal Note No. CBN/88-8, 1988 (unpublished); R. H. Siemann, CBN/89-2, 1989 (unpublished).
[16] Ph.D. thesis, S. Krishnagopal, 1991.
[17] R. Rossmanith and K. D. Cromer (unpublished).
[18] A. Gerasimov, CEBAF Report No. CEBAF-TN-90-243, 1990 (unpublished).
[19] R. Li, G. A. Krafft, and J. J. Bisognano (unpublished).
[20] Y. Baconnier, CERN Report No. CERN PS/91-02(LP), 1991 (unpublished).
[21] C. D. Johnson (unpublished).
[22] A. W. Chao, Stanford Linear Accelerator Center Report No. SLAC-PUB-3179, 1983 (unpublished).
[23] C. D. Johnson (private communication).
[24] C. K. Birdsall *et al.*, Methods Comput. Phys. **9**, 241 (1970).
[25] A similar result for round macroparticles has been obtained previously by G. A. Krafft.